Research Article

The Effects of Urbanization and Vegetation Cover on Urban Heat Island: A Case Study in Osmaniye Province

Deniz Çolakkadıoğlu [ID]

Department of Interior Architecture and Environmental Design, Faculty of Architecture, Design and Fine Arts, Osmaniye Korkut Ata University, Osmaniye TURKIYE

denizcolakkadioglu@osmaniye.edu.tr

Abstract

This study analyzed the changes in the urban heat island effect in the 30 years (from 1990 to 2021) in the central district of Osmaniye. In this sense, there were two primary goals. Firstly, Land use/land cover change (LULC), land surface temperature (LST), normalized difference built-up index (NDBI), and normalized difference vegetation index (NDVI) were analyzed by using remote sensing methods between 1990 and 2021. Secondly, a linear regression analysis was conducted to determine the factors associated with LST, NDVI, and NDBI. The study results revealed increases in urban surfaces and the average land surface temperature values in the past 30 years and showed a decline in the vegetation with low, medium, and high NDVI values. The regression analysis results indicated a strong negative relationship between LST and NDVI and a strong positive relationship between LST and NDBI. It was also found a robust negative relationship between NDBI and NDVI. In light of the findings, it was stated that the amount of open and green areas should be increased in order to prevent the negative effects of the urban heat island in the central district of Osmaniye. For this purpose, it has been proposed to encourage green roof systems throughout the city, to create city parks and to create a green belt system. In addition, as a result of the study, the importance of preventing forest destruction caused by over-settlement in the Amanos Mountains, which is one of the rare habitats of the world with different plant species, was emphasized. In this sense, legal sanctions should be employed to protect those areas and prevent construction.

Keywords: Land surface temperature (LST), Normalized difference built-up index (NDBI); Normalized difference vegetation index (NDVI), Urban heat island (UHI).

Introduction

Economic and industrial development and high population rates are closely associated with rapid changes in land uses/land cover change (LULC) in the 21st century, leading to the transformation of landscapes into residential areas and the increases in the amount of impervious surface worldwide. Impervious surfaces include buildings, roads, and industrial areas that absorb the short-wave solar radiation and reduce the long-wave solar energy emitted from the earth (Das et al., 2021). An increase in impervious surfaces results in warming the urban environment, creating the urban heat island (UHI) effect (Jamei et al., 2016).

The UHI effect is generally identified by using two methods. The first method involves the ground-based air temperature measurements in micro studies based on the modeling of meteorological data (Jamei et al., 2019). The second method is used in macro studies based on land surface temperature (LST) measurements. LST is measured through remote sensing methods using satellite image data and mapping the thermal energy released to the atmosphere from the earth. The LST measurements from thermal satellite images are easy, fast, continuous and very reliable as it allows calculating the energy emitted from the earth to the atmosphere (Celik et al., 2019; Atak and Tonyaloğlu, 2020).

Greenhouse gas emissions and LULC changes are the main factors affecting LST values (Sharma and Joshi, 2016; Koday and Kızılkan, 2019; Atak and Tonyaloğlu, 2020; Das et al. 2021; Das, 2022; Amadou and Arouna, 2022). Industrialization mainly depended on fossil fuels escalates greenhouse gas emissions, increasing the rate of greenhouse gases in the lower atmosphere (troposphere). The solar radiation reflected from the earth is absorbed and re-emitted in the troposphere and increases the surface temperature (Türkeş, 2012).

The radiation emissions from the earth's surface depend on the LULC changes. Impervious surfaces such as buildings and roads reflect radiation, but surfaces vegetation or covered with permeable materials absorb most radiation (Pal and Ziaul, 2017). Therefore, LULC changes affect LST values by changing the radiation absorption rates of the land surface (Atak and Tonyaloğlu, 2020).

Additionally, many studies emphasized that dense and healthy vegetation also affects the LST and UHI due to evaporation (Zhang et al., 2009; Malik et al., 2019). Thus, remote sensing techniques are applied to measure vegetation indices and to evaluate vegetation. One of those indices, the normalized difference vegetation index (NDVI), is widely used in many studies to describe vegetation patterns (e.g. Kumar and Shekhar, 2015; Guo

et al., 2015; Guha et al., 2018; Jamei et al. 2019; Philipps, et al., 2022). On the other hand, many researchers applied the normalized difference built-up index (NDBI) to investigate the effects of urban impervious surfaces such as roads and building roofs on LST (e.g. Zhang et al. 2009; Varshney, 2013; Guo et al. 2015; Alhawiti and Mitsova., 2016; Guha et al. 2018; Jamei et al. 2019; Malik et al. 2019). They stressed that the NDBI index, a measure to determine the residential areas by the changes in spectral reflections, is an important index to explore the relationships between urbanization and thermal stress. In addition, the studies on LST and UHI show that determining the factors affecting LST and the relationship between these factors is of great importance in the development of measures to reduce the urban heat island effect (e.g. Guo et al., 2015; Bakar et al., 2016; Das, 2022).

The study area, changed from county status to province status in 1996, and this administrative change led to significant demographic, industrial, and agricultural developments. It also influenced the LULC, especially the increasing urbanization. Forest areas, one of LULC's classes, were not an exception in this process. The forests of the Amanos Mountains, which is a very important area not only for Turkey but also for the world in terms of hosting plant species belonging to 3 phytogeographic regions, have been turning into impervious surfaces due to increasing transhumance activities.

In line with all these developments, it is of great importance to investigate the effects of changes in LST, NDVI and NDBI values in the central district of Osmaniye. Therefore, in this study, first of all, the effects of changes in LULC, LST, NDVI and NDBI values between 1990-2021 in the central district of Osmaniye were analyzed and, the change in the UHI effect was determined. Then, by exploring the relationships between LST, NDVI, and NDBI, suggestions were proposed to reduce the heat island effect.

Materials and Methods
Study area and data sets

Located in the east of the Mediterranean Region, Osmaniye is on the transition road between the east and west of Turkey. The Central Taurus Mountains surround Osmaniye from west to north and the Amanos Mountains from east to southeast (Figure 1). It is 3 279.9 km² and 121 m above sea level. Osmaniye was one of the districts of Adana until it became a province in 1996. Today it has seven districts. The central district-our study area has the highest population density and urbanization rate (274,420 residents).
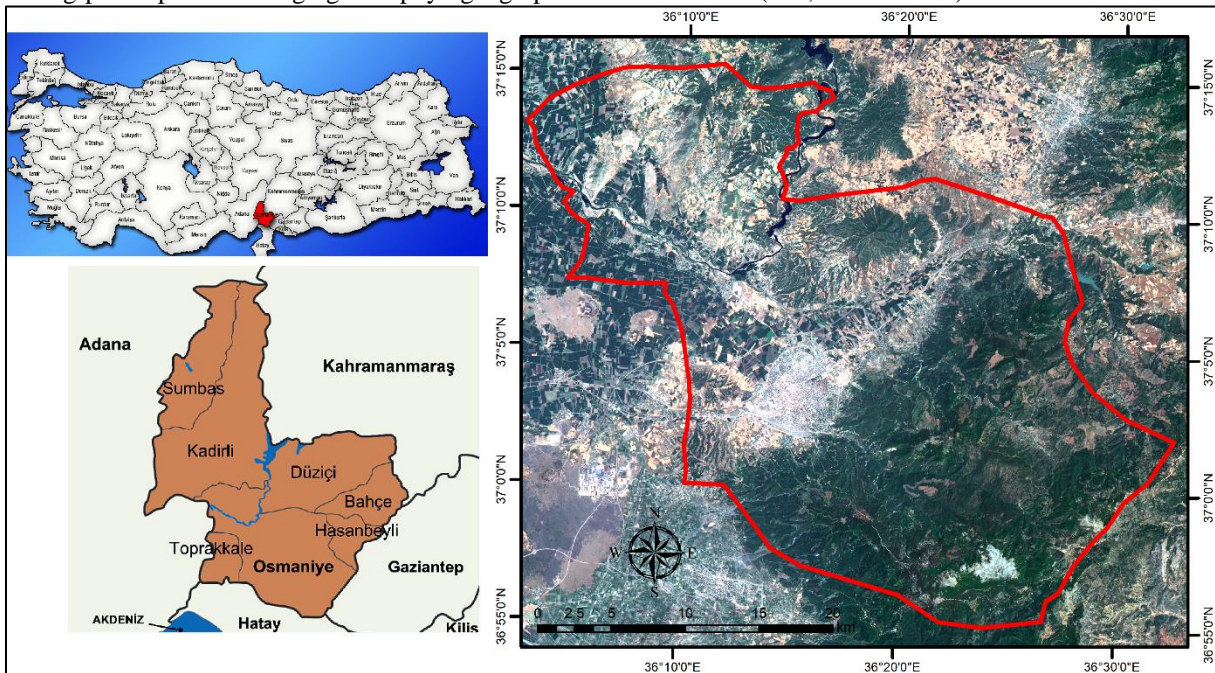
Fig.1. Location of the study area.

The study area has two different topographic structures: the northern plains and the southern mountainous. Although the climate differs between mountainous and plain areas, it mainly has Mediterranean climate characteristics characterized by generally mild and wet winters and hot and dry summers. Although there is a small amount of snowfall in the causeways and highland areas, there is no snowfall in the plains where summers are very hot, with an average temperature of 18.6 °C. The average highest temperature is 40 °C. Precipitation is high in winter and autumn, and the annual precipitation is 849.9 mm (General Directorate of Meteorology, 2021).

The northern part of the area is mainly plain covered by thick alluvial soils, which is the characteristic feature of the Çukurova region. In the study area, the Ceyhan River and its tributaries Horu Stream, Karaçay, Kesiksuyu Stream, Sabunsuyu Stream, and Savrun Stream facilitate irrigation expansion and increase agricultural productivity. Wheat, peanut, corn, sunflower, soybean, and radish are the primary agricultural products in the region. Besides, the production of olives for oil, oranges, and cher-

ries is also important. The city center is located on the southern border of the plain, but the topography changes towards the south, where the Amanos Mountains begin.

The Amanos Mountains have a rich vegetation diversity due to climatic and hydrological factors and soil conditions. As Aytaç and Semenderoğlu (2011) stated, the combination of topographic factors and geographical location have created suitable environments where the ecological requirements of the Mediterranean, Euro-Siberian, and Iran-Turan climates are met. Another rea-

son for the vegetation diversity is the Euro-Siberian penetrations through the high parts of the Amanos Mountains in the Mediterranean Region. Davis (1971) explains the Euro-Siberian penetrations through the Amanos Mountains with a migration route, known as *the Anatolian Diagonal*, a corridor between the North Anatolia and the Bolkar and Amanos Mountains (Figure 2). It indicated that plants migrated south through this corridor during the Pleistocene Glacial periods (Aytaç and Semenderoğlu, 2011).
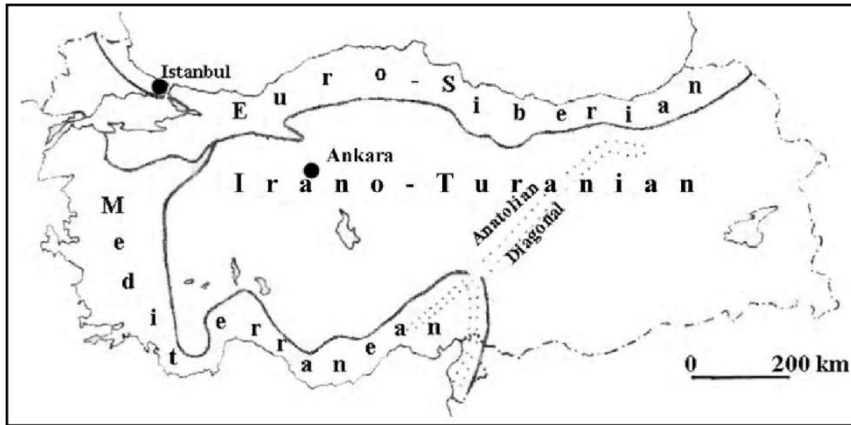
Fig.2. Phytogeography regions of Turkey and Anatolian diagonal (Gauquelin et al. 2016).

There are three vertical vegetation belts in the Amanos Mountains. The first belt is characterized by the maquis and is a secondary vegetation zone formed by the destruction of *Pinus brutia* forests, up to 700-800 m elevation. The dominant plant species in this belt include *Quercus coccifera, Myrtus communis, Phillyrea latifolia, Pistacia terebinthus, Calicotome villosa, Erica manipuliflora, Cotinus coggyria, Cistus* ssp., *Smilax aspera, Clematis cirrhosa,* and *Cercis siliquastrum*. The second vegetation zone is the Forest Belt, beginning from 120 m where the forest is not destroyed, or from the end of the maquis belt where forests are destroyed, ending at the highest forest boundary (1900 m). *Pinus brutia* up to 110 m, then mostly *Pinus nigra, Quercus cerris, and Fagus Orientalis* forms mixed stands. Lastly, the Upper Forest Belt starts from the end of the forest boundary (1900 m), and trees and shrubs cannot survive due to extreme climatic conditions in this zone. The ground is covered mainly by scrub shrubs (e.g., *Acantholimon libanoticum, Astragalus ssp., Asphodeline globifera, Asphodelus aestivus*) and alpine meadows (Provincial Environmental Status Report, 2019).

Amanos Mountains also has a vibrant wildlife habitat. For instance, the "Zorkun Wildlife Development Area," 3,889.85 hectares of forest area around the Zorkun Plateau, is used for breeding *Capreolus capreolus*. The other species in the protected area include mammals such as *Canis sp., Canis aureus, Sus* sp., *Vulpes vulpes, Hyaena sp., Lepus europaeus,* and *Erinaceus* sp.; raptors such as *Aegypius* sp. and *Aquila* sp. and birds such as *Grus grus, Alectoris* sp*.,* and *Coturnix* sp. (Tıraş and Besnek, 2017).

Data source and image preprocessing

In the study, the Landsat 5 Thematic Mapper (TM) and Landsat 8- Operational Land Imager (OLI) satellite images of 1990 and 2021 were used (Table 1). Both data were acquired from US Geological Survey Explorer. The data were inbuilt georeferenced to UTM zone 37 North projection with WGS-84 datum. Before the analysis, radiometric corrections and image enhancement procedures were executed with ArcGIS 10.7 software.

Table 1. The characteristics of the images.

Acquired Date	Acquired Time	Satellite	Sensor	Cloud Cover (%)	Sun Elevation (Degree)	Sun Azimuth (Degree)
21.08.1990	07:29:36	Landsat-5	TM	2.52	55.56	121.89
26.08.2021	08:09:18	Landsat-8	OLI	1.09	67.18	123.99

Classification of LULC

LULC maps were classified using the supervised classification method. The supervised classification was processed by ArcGIS 10.7. Bands 1-5 and 7 were used for

preparing LULC maps with Landsat 5 –TM images, but the 6 was excluded because it was a thermal band. The bands 1-7 were considered for Landsat 8-OLI images. All the bands were compounded in ArcGIS 10.7 software using the image analyst tool, and then data were

corrected for radiometric and atmospheric distortions. Landsat 8 imagery with a spatial resolution of 30m was pan-sharpened using the ESRI method with the 15m panchromatic bands for better LULC classification. More than 200 training samples were collected randomly using the training sample manager tool. The LULC of the study area was categorized into 5 group: building area, vegetation, agricultural lands, water body, and bare lands.

Calculation of NDVI

NDVI describes the vegetation proportion by measuring the difference in the near-infrared portion of the electromagnetic spectrum and red portion of the spectrum (Aygün et al. 2016; Malik et al. 2019). Healthy and lush vegetation absorbs visible light and reflects most of the near-infrared light. On the contrary, unhealthy vegetation condition reflects more visible light and less near-infrared light. NDVI has values ranging from +1 to -1 (+1 for the healthy vegetation and -1 for areas with no vegetation).

NDVI was calculated in ArcGIS 10.7 using NIR Band 5 and Red Band 4 of the Landsat-8 data and NIR Band 4 and RED Band 3 of the Landsat-5 data as shown in the equation below (Rogan et al. 2013; Kikon et al. 2016).

$$NDVI = \frac{NIR - R}{NIR + R}$$

Calculation of NDBI

NDBI ranges from -1 to +1 and distinguishes built-up territory from other land uses/land surfaces. Built-up lands have higher reflectance in MIR than in NIR. Therefore, the high NDBI values show the built-up areas.
NDBI was calculated in ArcGIS 10.7 software using MIR Band 6 and NIR Band 5 of the Landsat-8 data and MIR Band 5 and NIR band 4 of Landsat-5 data as shown in the equation (1) (Zha et al., 2003).

$$NDBI = \frac{MIR - NIR}{MIR + NIR} \tag{1}$$

Calculation of LST

LST refers to the temperature measured by the remote sensor (Jin et al., 2011; Sutariya et al., 2022). As the LST provides essential data about a climate system, the procedure has been addressed and clarified in many studies (e.g., Xiong et al., 2012; Asgarian et al., 2014; Xu and Zhang, 2017; Roy et al. 2020).
In this study, the Landsat 5 images for 1990 and Landsat 8 images for 2021 were used to perform the LST analysis described below:

Step 1: Conversion to Top of Atmosphere (TOA) Radiance: we applied the formula in equation (2) to convert Thermal Infra-Red Numbers (DN) to TOA values for Landsat-8 data (USGS, 2019).

$$TOA = ML * band\ 10 + F - Oj \tag{2}$$

ML = the band-specific multiplicative rescaling factor= 0.0003342
F = re-scaling factor = 0.1
O_j = correction value =0.29.

The formula in equation (3) was applied to the Landsat-5 TM data.

$$TOA = \left(\frac{LMAX\lambda - LMIN\lambda}{QCALMAX - QCALMIN}\right) * (band\ 6 - QCALMIN) + LMIN\lambda \tag{3}$$

$L_{MAX\lambda}$= It is the radiance that is scaled to $QCAL_{MAX}$
$L_{MIN\lambda}$= It is the radiance that is scaled to $QCAL_{MIN}$
Q_{CALMIN}= It is the lowest calibrated value LMINλ
Q_{CALMAX}= It is the highest calibrated value LMAX λ

Step 2: Brightness Temperature: Radiance values were converted to brightness temperature using equation (4) (USGS, 2019).

$$T = \frac{K2}{\left(\frac{K1}{TOA}\right) + 1} - 273.15 \tag{4}$$

T= Brightness temperature (^{0}C)
K$_1$=Calibration constant 1 (Table 2)
K$_2$= Calibration constant 2 (Table 2)

Table 2. Thermal constant of Landsat TM and OLI thermal imageries.

Sensor	Year	Band	Constant 1 K$_1$ (Watts/(m^2*sr*µm))	Constant 2 K$_2$ (Kelvin)
Landsat 5	1990	Band 6	607.76	1260.56
Landsat 8	2021	Band 10	774.89	1321.08

Step 3: Calculation of LST applying the equation (5) (USGS 2019).

$$LST = \frac{T}{\left[1 + \left\{\left(\frac{\lambda * T}{c}\right) * InE\right\}\right]} \tag{5}$$

T= Brightness temperature (^{0}C)
λ= Wavelength of emitted radiance =10.8 for band 10
E= Emissivity of land surface
C=14388mK

It is necessary to obtain the Land surface emissivity (E) to calculate the LST. It refers to the radiating and ab-

sorbing power of a surface in the long-wave radiation spectrum and generally differs by the land cover characteristics (Sobrino et al., 2008). The equation is shown below (Weng et al. 2004; Sobrino et al. 2004):

$$E = 0.004 * Pv + 0.986 \tag{6}$$

E= Land surface emissivity
Pv= Proportion of vegetation
0.986 is the correction value

To determine the land surface emissivity (E) value, the vegetation proportion (Pv) parameter equation proposed

by Carlson and Ripley (1997) is shown below (USGS, 2019):

$$Pv = (((NDVI - NDVImin))/((NDVImax - NDVImin)))^2 \quad (7)$$

Pv= Vegetation proportion
NDVI$_{min}$= It is the lowest value of NDVI
NDVI$_{max}$= It is the highest value of NDVI

Statistical analysis

In the study, linear regression analysis was performed to reveal the relationship between LST and NDVI, LST and NDBI, and NDVI and NDBI, as in many other studies (e.g. Guo et al. 2015; Bakar, 2016; Roy et al. 2020; Das, et al. 2021). Therefore, all pixels were converted to points. Then, the parameter values of these points were obtained from the LST, NDVI and NDBI maps and shown in graphics.

Results and Discussions
Land use and land cover change

The land use of Osmaniye central district was categorized into five: water surface, vegetation, bare lands, agricultural lands, and built-up. Figure 3 shows the spatial distribution of land use in Osmaniye in 1990 and 2021.
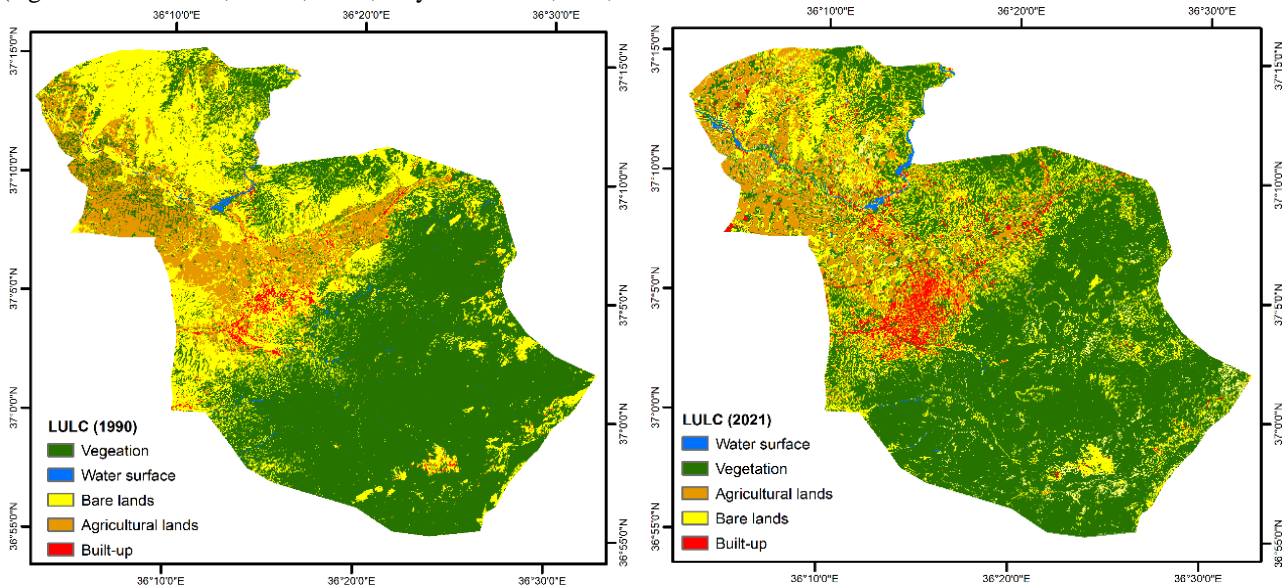
Fig. 3. Spatial distribution of LULC in 1990 and 2021.

Table 3. LULC and change statistics of Osmaniye

Land type	year 1990		year 2021		Change in the period of 1990 and 2021	
	ha	%	ha	%	ha	%
Water surface	486.6	0.54	490.59	0.55	+3.99	+0.82
Built-Up	1 466.88	1.63	3 787.70	4.21	+2 320.82	+158.21
Vegetation	50 626.06	56.3	48 938.87	54.43	- 1 687.19	-3.33
Agricultural lands	10 244.23	11.39	13 368.51	14.87	+3 124.28	+30.50
Bare lands	27 094.34	30.13	23 332.44	25.95	-3 761.90	-13.88
Total	89 918.11	100	89 918.11	100	-	-

Table 3 presents the LULC and change statics. The (-) minus sign indicates that it has decreased compared to the previous period, and the (+) plus sign indicates the opposite. The analysis results showed that between 1990-2021, built-up areas increased significantly from 1. 466.88 ha to 3 787.70 ha by 158%, but bare lands and vegetation decreased. There was a significant increase of 30% in the number of agricultural lands.

The land use maps provide essential information about the spatial change in urban regions. In the 1990s, single or two-story buildings with gardens were mainly located very close to agricultural lands. However, after the 2000s, the rate of multi-story construction increased, and the city center was spatially separated from agricultural areas. As seen in Figure 3, the built-up area has spatially expanded to the east of Osmaniye between 1990 to 2021. Although the number of agricultural lands in the city increased, it indirectly led to a decrease in vegetation cover. The primary reason for the reduction in vegetation is the destruction of green areas to open up new agricultural areas. Another reason was the increase in the upland settlement around densely covered vegetation.

Due to the high temperatures, especially in summer, a significant proportion of the urban population lives in upland settlements in the Amanos Mountains, where the weather is colder than the city center between May and October. There are many upland settlements in the vegetation of the Amanos Mountains in the south of Osmaniye. Therefore, the increasing population in such settlements has destroyed the rich and unique vegetation of the Amanos Mountains.
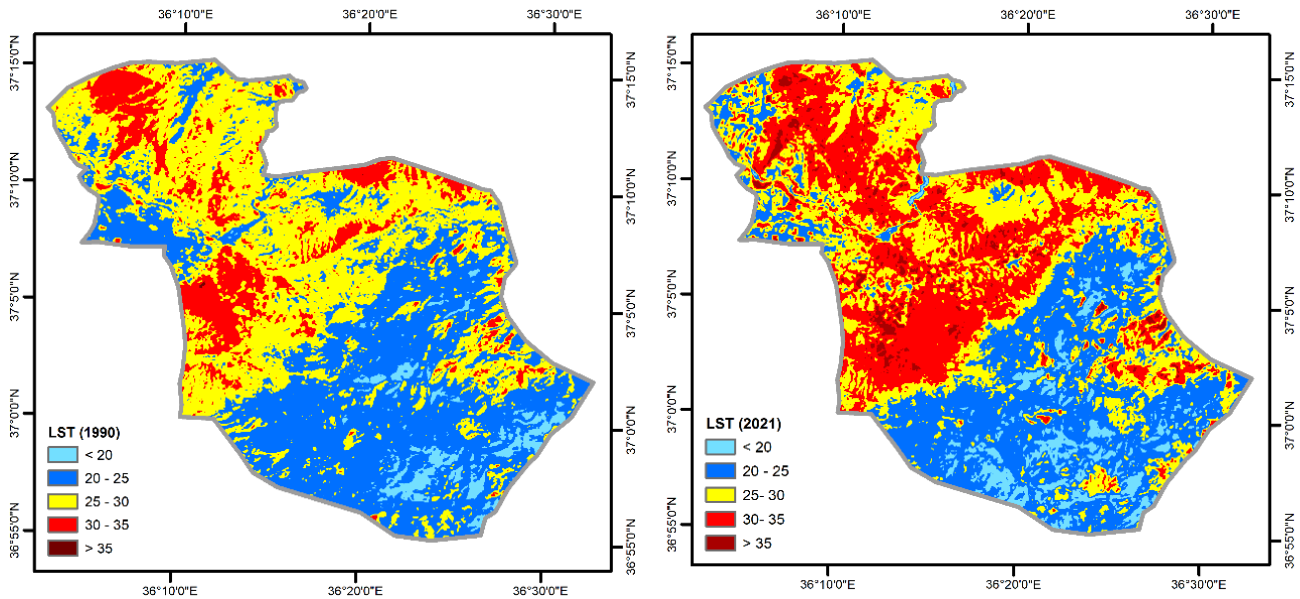
Fig. 4. LST maps for the years 1990 and 2021.

LST

Figure 4 shows the LST maps of the study area in 1990 and 2021. As seen in the figure, the average temperature in the southern part of Osmaniye was 20-25 ^{0}C in the 1990s; it rose to 30-35 ^{0}C in this region in 2021 (see Figure 3 and Figure 4). Similarly, there is a significant increase in urban settlements' LST values. Table 4 shows a statistical overview of LST values. In general, there has been an increase in the maximum and average temperature values of the study area over the 30 years. The average temperature rose from 25.72 ^{0}C to 27.00 ^{0}C. Findings from this study show similar results with other studies investigating the relationship between land use change and LST (e.g. Xiong et al., 2012; Sahebjalal and Dashtekian, 2013; Alhawiti and Mitsova, 2016; Sharma and Joshi, 2016; Bakar et al., 2016; Roy et al., 2020; Das et al., 2021).

Table 4. A statistical overview of the LST values for Osmaniye City

	Min.	Max.	Average	Standard deviation
1990	16.56	36.44	25.72	0.37
2021	16.47	40.56	27.00	0.59

NDVI

The normalized difference vegetation index (NDVI) identifies and monitors vegetation (Sahebjalal and Dashtekian, 2013; Malik et al., 2019; Akyürek, 2020; Maskooni et al. 2021). Several studies also investigate the effects of NDVI on the urban heat island (UHI) (e.g. Li et al., 2009; Petropoulos et al. 2014; Kumar and Shekhar, 2015; Jamei et al. 2019; Malik et al., 2019; Maskooni et al. 2021). Negative NDVI values correspond to the water surface, and the values close to zero to the soil, bare lands, or residential areas. As the Petropoulos et al. (2014) stated that the values between 0.1 and 0.75 generally indicate vegetation cover.

NDVI maps are shown in Figure 5. The lowest values showed bare lands and buildings. However, as emphasized by Khanal et al. (2019), Ma et al. (2019), and Maskooni et al. (2021), it is tough to distinguish bare lands and built-up areas by using NDVI values. The NDVI value of above 0.1 corresponds to the vegetation cover. Similarly, as Sahebjalal and Dashtekian (2013), in this study, the values of NDVI were categorized as low (0.1 - 0.2), medium (0.2 - 0.3), high (0.3- 0.4), and very high (0.4-…). As shown in Figure 5, the most drastic changes mainly occurred in three regions. The first region was the Osmaniye city center, where NDVI values decreased significantly. The changes in the agricultural lands in the north and the highland settlements in the south were also evident. Especially the upland settlements in the Amanos Mountains, which have rich vegetation cover, led to a decline in vegetation across the study area.

Table 5 shows the NDVI density classes in 1990 and 2021, and Table 6 gives a statistical summary of NDVI values. As shown in Table 5, there were decreases in low, medium, and high-density classes, but a very high increase occurred in built-up areas.
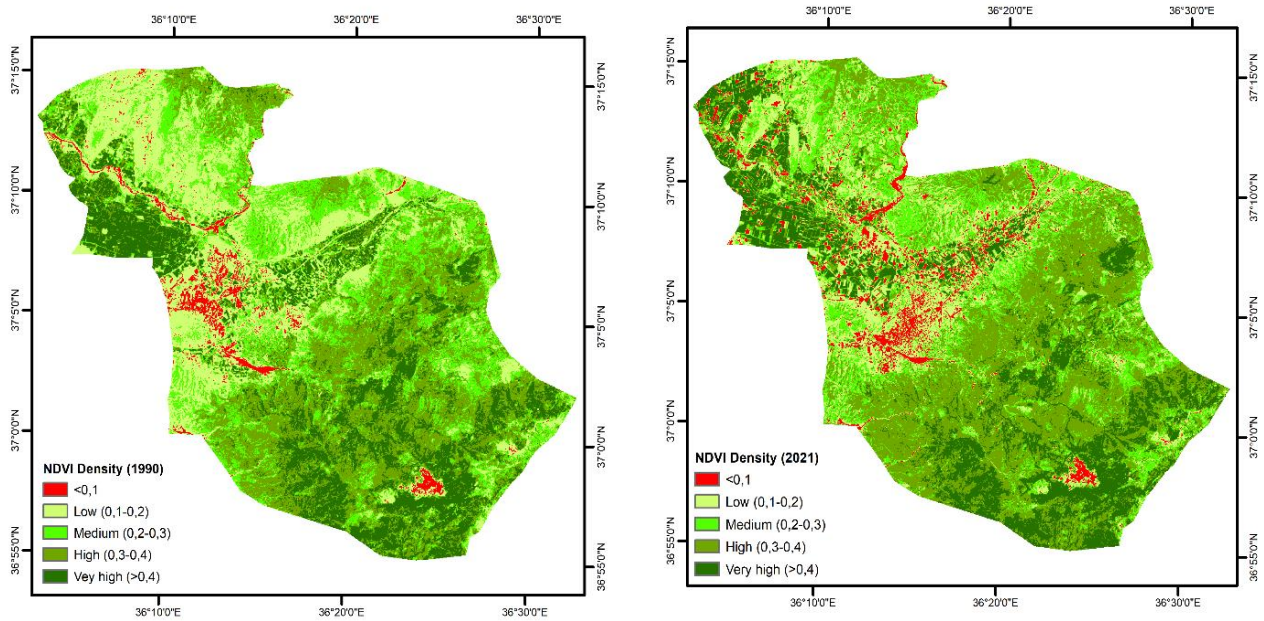
Fig. 5. NDVI density map of 1990 and 2021.

Table 5. The NDVI density classes between 1990 and 2021.

	year 1990		year 2021		From the year 1990 to year 2021	
	ha	%	ha	%	ha	%
<0.1	2 273.77	2.50	4 597.96	5.13	+2 324.19	+102.21
Low (0.1-0.2)	21 945.27	24.45	20 479.93	22.77	-1 465.34	-6.67
Medium (0.2-0.3)	19 976.66	22.21	18 942.73	21.06	-1 033.93	-5.17
High (0.3-0.4)	28 802.85	32.03	29 592.86	32.91	+790.01	+2.74
Very high (>0.4)	16 919.59	18.81	16 304.66	18.13	-614.93	-3.63
Total	89 918.14	100	89 918.14	100	-	-

Table 6. The statistical summary of NDVI values for Osmaniye City.

	Min.	Max.	Average	Standard deviation
1990	-0.24	0.62	0.21	0.13
2021	-0.15	0.61	0.32	0.12

NDBI

NDBI has been applied in many studies as it helps distinguish the built-up areas from other land uses and land cover (Zha et al., 2003; Chen et al., 2006). The NDBI density maps are given in Figure 6 and statistical data are shown in Table 7. Ranagalage et al. (2018) stated that the negative NDBI values correspond to vegetation, small positive values to bare lands, and significant positive values to built-up areas. However, the NDBI values indicating residential differed in some studies (e.g. Xu and Zhang 2017; Jamei et al. 2019; Balew and Korme 2020; Maskooni et al., 2021). In this study, the NDBI value representing the built up areas was 0.09 for the year 1990 and, 0.12 for the year 2021. The reason for such an increase in NDBI value was the decline in vegetation and the increase in residential areas, which overlaps with the findings of Maskooni et al. (2021).

Table 7. A statistical summary of NDBI values for Osmaniye City

	Min.	Max.	Average	Standard deviation
1990	-0.25	0.41	0.08	0.13
2021	-0.43	0.36	-0.16	0.11
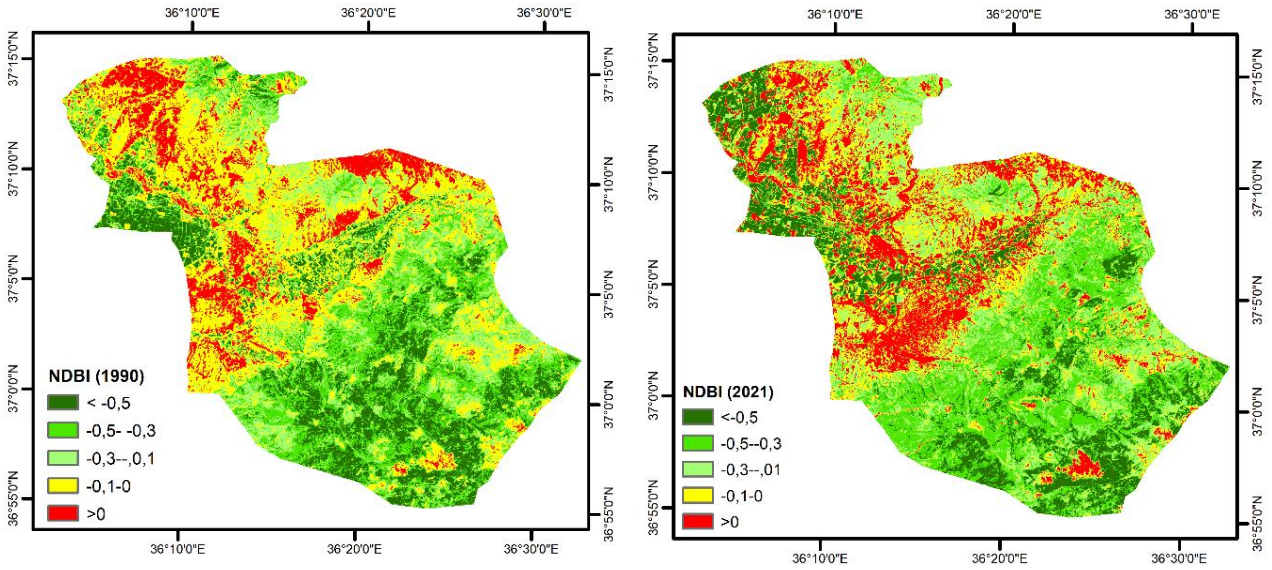
Fig. 6. NDBI density map in 1990 and 2021.
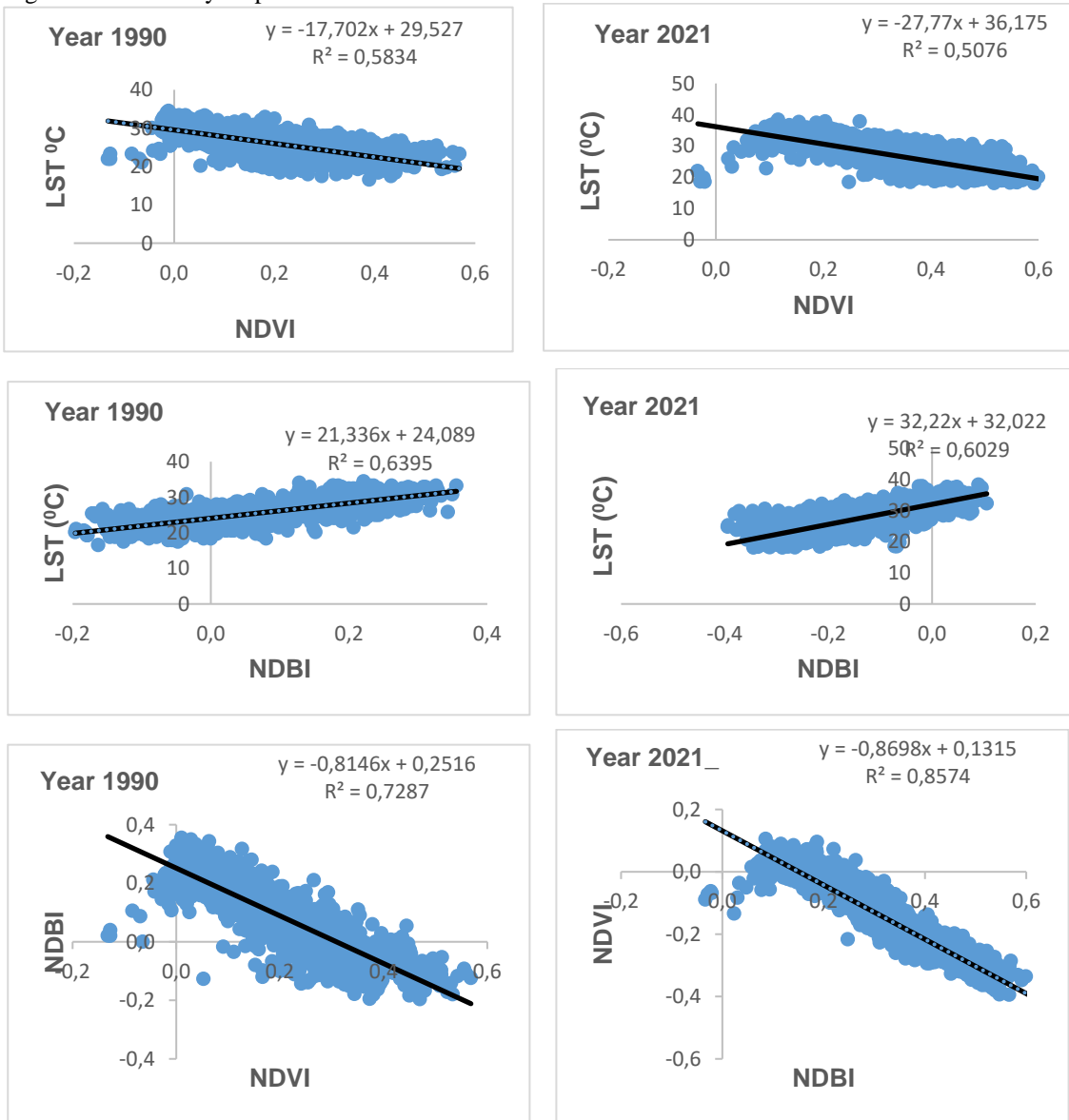
Fig. 7. Relationship of LST vs. NDVI, LST vs NDBI and NDVI vs. NDBI.

Table 8. Correlation matrix of the parameters

the year 1990				the year 2021			
	LST	NDVI	NDBI		LST	NDVI	NDBI
LST	1	-0.5834	0.6395	**LST**	1	-0.5076	0.6029
NDVI	-0.5834	1	-0.7287	**NDVI**	-0.5076	1	-0.8574
NDBI	0.6395	-0.7287	1	**NDBI**	0.6029	-0.8574	1

The Relationship of LST vs. NDVI, LST vs. NDBI and NDVI vs. NDBI

The correlations between LST and NDVI, LST and NDBI, NDBI and NDVI are shown in Figure 7. The value matrix is presented in Table 8.

As seen in the figure above, there is a negative relationship between NDVI and LST values between 1990 and 2021. Similarly, several studies conducted in different countries concluded that the land surface temperature increased with the decreases in the vegetation cover (e.g. Zhang et al., 2009; Kumar and Shekhar, 2015; Alhawiti and Mitsova, 2016; Sharma and Joshi, 2016; Guha et al., 2018; Malik et al., 2019; Maskooni et. al. 2021).

In this study, it was also examined how the changes in NDBI affected the NDVI values. As a result, it was determined that there is a negative relationship between NDBI and NDVI. Roy et al. (2020) similarly indicated that the growth of urban areas led the green areas to turn into gray/constructed areas.

Conclusion

In this study, LST values of 1990 and 2021 were analyzed in order to determine the change in the urban heat effect in Osmaniye over 30 years. The study results showed that the average temperature of Osmaniye city was 25^0C in 1990, but it rose to 27^0C in 30 years. In order to determine the spatial changes in the LST values, LULCC maps for 1990 and 2021 were formed.

As a result of the LULCC maps, it was found that the land use of Osmaniye district had changed rapidly from 1990 to 2021 due to urbanization and agricultural and industrial practices. It mainly stemmed from the administrative change in Osmaniye, which used to be a district of Adana until 1996. It was governed as a province after 1996. The governance shift has led to the construction of multi-story buildings in the city center, where there used to be single or two-story structures closely located near agricultural lands. The residential areas have been completely separated from the agricultural lands and expanded towards the east of our study area, which resulted in a 158% increase in impervious surfaces. Besides, the increasing population in upland areas has destroyed the forests in the Amanos Mountains, which have rich flora.

When considering the LULCC and the increasing LST in Osmaniye, it was found that the highest temperature increases experienced in impermeable surfaces such as urban areas and bare lands. It showed that LST was correlated with LULC. A description of the correlations between LST and ground surface characteristics allows us to take effective measures to reduce the UHI effect. Therefore, it was also aimed to determine the factors related to the LST. For this purpose, NDVI and NDBI analysis were performed and made a linear regression analysis to describe LST correlations.

The study results showed a negative relationship between LST and NDVI, implying that the land surface temperature was lower in surfaces with dense vegetation. It was a strong negative relationship: R^2=-0,5834 and R^2=-0,5076 for the years 1990 and 2021, respectively. The significant negative correlation between NDVI and LST indicates that healthy vegetation lowers the surface temperature.

A strong positive correlation between LST and NDBI was determined, which justifies higher temperature values in dense urban areas and bare lands. Also strong negative correlation between NDBI and NDVI was determined in this study.

As similarly emphasized in some studies (e.g. Weng et al. 2004; Huang et al. 2008; Sahebjalal and Dashtekia, 2013; Ahmad et al. 2022), the attempts to increase the vegetation cover would be simple but effective measures to limit the UHI effect and prevent the harmful consequences of climate change. Hence, in order to reduce the negative effects of UHI in the central district of Osmaniye, urban green areas should be increased, green roof systems should be encouraged and the green belt approach should be adopted throughout the city.

Amanos Mountains are one of the rare regions in the world rich in plant species and diversity in addition to the relict and endemic species such as *Pinus brutia* and *Fagus orientalis*, which have significantly different ecological demands. Therefore, as Aytaç and Semenderoğlu (2011) stated, forest destruction due to the increasing upland settlements in the Amanos Mountains should be prevented. The wildlife protection area status is not legally sufficient to prevent excessive construction in the region. Thus, a protected area status that would not allow construction or limit construction in such areas should be declared to protect the area.

References

Ahmad, N., Waqas, T., Shafique, M., Khattak, I. (2022). The land surface temperature dynamics and its impact on land cover in district Peshawar, Khyber Pakhtunkhwa, *International Journal of Environment and Geoinformatics* (IJEGEO), 9(3): 097-107, doi. 10.30897/ijegeo. 890206

Akyürek, Ö. (2020). Determination of Surface Temperatures with Thermal Remote Sensing Images: A Case Study of Kocaeli, Artvin Coruh University. Natural Disasters Application, and Research Center *Journal of Natural Hazards and Environment*. 6(2): 377-390. doi:10.21324/dacd.667594.

Alhawiti, R. H., Mitsova, D. (2016). Using landsat-8 data to explore the correlation between urban heat island and urban land uses. IJRET: *International Journal of Research in Engineering and Technology* 5(3): 457-466. eISSN: 2319-1163 pISSN: 2321-7308. *http://www.ijret.org.*

Amadou,I., Arouna, O. (2022). Estimation of Greenhouse Gas Emissions from Remote Sensing and Field Data in the Wari-Maro Forest Reserve and Its Periphery (Benin). *International Journal of Environment and Geoinformatics*, 9(3), 73-83, doi. 10.30897/ijegeo.1023286

Asgarian, A., Amiri, B., Sakieh, Y. (2014). Assessing the effect of green cover spatial patterns on urban land surface temperature using landscape metrics approach. *Urban Ecosyst.* 18: 209–222. doi:10.1007/s11252-014-0387-7.

Aygün, C., Sever, A. L.,. İsmail, K.A.R.A., Erdoğdu, İ., Atalay, A.K. (2016). Use of NDVI Data on Planning of Grazing in Eskisehir Grasslands. *Journal of Field Crops Central Research Institute*, 25(1).

Aytaç, A.S., and Semenderoğlu, A. (2011) . Vegetation geography of the central part of the Amanos Mountains. *Journal of Anatolian Natural Sciences*, 2(2): 34-47.

Bakar, S.B., Pradhan, B., Lay, U.S., Abdullahi, S. (2016). Spatial assessment of land surface temperature and land use/land cover in Langkawi Island. 8th IGRSM International Conference and Exhibition on Remote Sensing & GIS (IGRSM 2016), IOP Conf. Series: *Earth and Environmental Science* 37 (2016) 012064. doi: 10.1088/1755-1315/37/1/012064.

Balew, A., Korme, T. (2020). Monitoring land surface temperature in Bahir Dar City and its surrounding using Landsat images. *The Egyptian Journal of Remote Sensing and Space Science*. doi:10.1016/j.ejrs.2020.02.001.

Carlson, T., Ripley, D. A. (1997). On the relation between NDVI, fractional vegetation cover, and leaf area index. *Remote Sensing of Environment*, 62(3): 241-252.doi: 10.1016/S0034-4257(97)00104-1.

Celik, B., Kaya, Ş., Alganci, U., Seker, DZ. (2019). Assessment of the relationship between land use/cover changes and land surface temperatures: a case study of thermal remote sensing, *FEB Fresenius Environ. Bull.,*3, 541

Chen, X., Zhao, H., Li, P., Yin, Z. (2006). Remote sensing image-based analysis of the relationship between urban heat island and land use/cover changes. *Remote Sensing of Environment*, 104(2):133-146. Doi:10.1016/j.rse.2005.11.016.

Das, N., Mondal, P., Sutradhar, S., Ghosh, R. (2021). Assessment of variation of land use/land cover and its impact on land surface temperature of Asansol subdivision. *The Egyptian Journal of Remote Sensing and Space Sciences*, 24(1): 131-149. doi: 10.1016/j.ejrs.2020.05.001.

Das, S. (2022). A Review of UHI formation over changing climate and its impacts on Urban Land Use and Environments and Adaptation Measures. International *Journal of Environment and Geoinformatics* (IJEGEO), 9(1): 064-073. doi. 10.30897/ijegeo.938231

Gauquelin, T., Michon, G., Joffre, R., Duponnois, R., Génin, D., Fady, B., Dagher-Kharrat, M.B., Derridj, A., Slimani, S., Badri, W., Alifriqui, M., Auclair, L., Simenel, R., Aderghal, M., Baudoin, E., Galiana, A., Prin, Y., Sanguin, H., Fernandez, C., Baldy, V. (2016). Mediterranean forests, land use and climate change: a social-ecological perspective. *Regional Environmental Change*, 18*:* 623-636.doi: 10.1007/s10113-016-0994-3.

General Directorate of Meteorology. (2021). T.R. Ministry of Agriculture and Forestry, General Directorate of Meteorology 1987-2020 data.https://www.mgm.gov.tr/veridegerlendirme/il-ve-ilceler-istatistik.aspx?m=OSMANIYE (accessed 11/03/2021).

Guha, S., Govil, H., Dey, A., Gill, N. (2018). Analytical study of land surface temperature with NDVI and NDBI using Landsat 8 OLI and TIRS data in Florence and Naples City, Italy. *European Journal of Remote Sensing* 51 (1): 667–678. doi: 10.1080/22797254.2018.1474494.

Guo, G., Wu, Z., Xio, R., Chen, Y., Liu, X., Zhang, X. (2015). Impacts of urban biophysical composition on land surface temperature in urban heat island clusters. *Landscape and Urban Planning* 135 (2015): 1–10. Doi: 10.1016/j.landurbplan.2014.11.007.

Huang, L., Zhao, D., Wang, J., Zhu, J., Li, J. (2008). Scale impacts of land cover and vegetation corridors on urban thermal behavior in Nanjing, China. *Theoretical and Applied Climatology*, 94(3-4): 241-257.doi: 10.1007/s00704-007-0359-4.

Jamei, E., Rajagopalan, P., Seyedmahmoudian, M., Jamei, Y. (2016). Review on the impact of urban geometry and pedestrian level greening on outdoor thermal comfort. *Renewable and Sustainable Energy Reviews* 54: 1002–1017. Doi: 10.1016/j.rser.2015.10.104.

Jamei, Y., Rajagopalan, P., Sun, Q. (2019). Spatial structure of surface urban heat island and its relationship with vegetation and built-up areas in Melbourne, Australia. *Science of the Total Environment* 659 (2019): 1335–1351. doi: 10.1016/j.scitotenv.2018.12.308.

Jin, M.S., Kessomkiat, W., Pereira, G. (2011). Satellite-observed urbanization characters in Shanghai, China: aerosols, urban heat island effect, and land–atmosphere interactions. *Remote Sensing*, 3(1): 83-99. Doi:10.3390/rs3010083.

Kesgin Atak, B., Ersoy Tonyaloğlu, E. (2020). Evaluation of the effect of land use/land cover and vegetation cover change on land surface temperature: The case of Aydın province. *Turkish Journal of Forestry*, 21(4): 489- 497. Doi: 10.18182/tjf.786827.

Khanal, N., Uddin, K., Matin, M., Tenneson, K. (2019). Automatic Detection of Spatiotemporal Urban Expansion Patterns by Fusing OSM and Landsat Data in Kathmandu. *Remote Sensing* 11 (19): 2296.doi: 10.3390/rs11192296.

Kikon, N., Singh, P., Singh, S.K., Vyas, A. (2016). Assessment of urban heat islands (UHI) of Noida City, India using multi-temporal satellite data. *Sustainable Cities and Society*. 22: 19–28. doi:10.1016/J.SCS.2016.01.005.

Koday, S., Kızılkan, Y. (2019). Determining the Changes in the use of the Lands in Unye District through the LULC and NDVI Analyses by means of multi-time Landsat satellite imaging. Journal of *Atatürk University Institute of Social Sciences*, 23 (3): 1301-1312.

Kumar, D., Shekhar, S. (2015). Statistical analysis and surface temperature–vegetation indexes relationship through thermal remote sensing. *Ecotoxicology and Environmental Safety*, 121(2015): 39-44. doi: 10.1016/j.ecoenv.2015.07.004.

Li, J., Wang, X., Wang, X., Ma, W. (2009). Remote sensing evaluation of urban heat island and its spatial pattern of the Shanghai metropolitan area, China. *Ecological Complexity*, 6(4): 413–420. Doi: 10.1016/j.ecocom.2009.02.002.

Ma, X., Li, C., Tong, X., Liu, S. (2019). A new fusion approach for extracting urban built-up areas from multisource remotely sensed data. *Remote Sensing* 11 (21): 2516. doi: 10.3390/rs11212516.

Malik, M.S., Shukla, J.P., Mishra, S. (2019). Relationship of LST, NDBI and NDVI using Landsat-8 data in Kandaihimmat Watershed, Hoshangabad, India. *Indian Journal of Geo Marine Sciences*, 48 (01): 25-31.

Maskooni, E.K., Hashemi, H., Berndtsson, R., Arasteh, P.D., M. Kazemi. (2021). Impact of spatio temporal land-use and land cover changes on surface urban heat islands in a semi arid region using Landsat data. *International Journal of Digital Earth*, 14(2): 250-270, doi:10.1080/17538947.2020.1813210.

Pal, S., Ziaul, S.K. (2017). Detection of land use and land cover change and land surface temperature in English Bazar urban centre. *The Egyptian Journal of Remote Sensing and Space Science*, 20(1): 125-145. doi: 10.1016/j.ejrs.2016.11.003

Petropoulos, G.P., Griffiths, H.M., Kalivas, D.P. (2014). Quantifying spatial and temporal vegetation recovery dynamics following a wildfire event in a Mediterranean landscape using EO data and GIS. *Applied Geography*, 50:120–131. doi:10.1016/j.apgeog.2014.02.006.

Philipps, N., Landes, T., Kastendeuch, P., Najjar, G., Gourguechon, C. (2022). Urban Heat Island Mapping Based on a Local Climate Zone Classification :A Case Study in Strasbourg City, France. *International Journal of Environment and Geoinformatics,* 9(4), 57-67 ,doi.10.30897/ijegeo.1080023

Provincial Environmental Status Report Osmaniye. (2019). Osmaniye Governorship Provincial Directorate of Environment and Urbanization, Department of EIA, and Environmental Permits. pp:212. https://webdosya.csb.gov.tr/db/ced/icerikler/osmanye_2018_-cdr_son-20190828111313.pdf.

Ranagalage, M., Estoque, R.C., Zhang, X., Murayama, Y. (2018). Spatial changes of urban heat island formation in the Colombo District, Sri Lanka: Implications for sustainability planning. *Sustainability*, 10(5): 1367. doi: 10.3390/su10051367.

Rogan, J., Ziemer, M., Martin, D., Ratick, S., Cuba, N., DeLauer, V. (2013). The impact of tree cover loss on land surface temperature: A case study of central Massachusetts using Landsat Thematic Mapper

thermal data. *Applied Geography*, 45: 49–57. doi: 10.1016/j.apgeog.2013.07.004.

Roy, S., Pandit, S., Eva, E.A. S., Bagmar, H., Papia, M., Banik, L., Dube, T., Rahman, F., Razi, M.A. (2020). Examining the nexus between land surface temperature and urban growth in Chattogram Metropolitan Area of Bangladesh using long term Landsat series data. *Urban Climate* 32 (2020) 100593. doi: 10.1016/j.uclim.2020.100593.

Sahebjalal, E., Dashtekian, K. (2013). Analysis of land use-land covers changes using normalized difference vegetation index (NDVI) differencing and classification methods. *African Journal of Agricultural*, 8(37): 4614-4622. doi: 10.5897/AJAR11.1825.

Sharma, R., Joshi, P.K. (2016). Mapping environmental impacts of rapid urbanization in the National Capital Region of India using remote sensing inputs. *Urban Climate*, 15(2016): 70-82. doi:10.1016/j.uclim.2016.01.004.

Sobrino, J.A., Jiménez-Muñoz, J.C., Paolini, L. (2004). Land surface temperature retrieval from Landsat TM 5. *Remote Sensing of Environment,* 90: 434–440. doi: 10.1016/j.rse.2004.02.003.

Sobrino, J.A., Jimenez-Muoz, J.C., Soria, G., Romaguera, M., Guanter, L., Moreno, J., Plaza, A., Martinez, P. (2008). Land surface emissivity retrieval from different VNIR and TIR sensors. *Transactions on Geoscience and Remote Sensing*, 46(2): 316-327. Doi: 10.1109/TGRS.2007.904834.

Sutariya, S., Hirapara, A., Tiwari, M. K., (2022). Development of Modeler for Automated Mapping of Land Surface Temperature Using GIS and LANDSAT8 Satellite Imagery. *International Journal of Environment and Geoinformatics* (IJEGEO), 9(2):054-059, doi. 10.30897/ijegeo.820906

Tıraş, M., Besnek, F. (2017). A tourism potential of Osmaniye. Ataturk University, *Journal of Social Sciences Institute*, June (2017), 21 (2): 757-777.

Türkeş, M. (2012). Observed and projected climate change, drought, and desertification in Turkey. Ankara University Journal of *Environmental Sciences* 4(2): 1-32. doi:10.1501/Csaum_0000000063.

USGS. (2019). United States Geological Survey (USGS). Landsat 8 (L8) Data Users Handbook, LSDS-1574.2019. Version 5.0, URL: http://landsat.usgs.gov/Landsat8_Using_Product.php (accessed 11/08/2021).

Varshney, A. (2013). Improved NDBI differencing algorithm for built-up regions change detection from remote-sensing data: an automated approach. *Remote Sensing Letters*, 4(5): 504-512. doi: 10.1080/2150704X.2013.763297.

WBPCB (2019). Final report on Waste Inventory (MSW & BMW).

Weng, Q., Lu, D., Schubring, J. (2004). Estimation of land surface temperature-vegetation abundance relationship for urban heat island studies. *Remote Sensing of Environment*, 89(4): 467–483. doi: 10.1016/j.rse.2003.11.005.

Xiong, Y., Huang, S., Chen, F., Ye, H., Wang, C., Zhu, C. (2012). The impacts of rapid urbanization on the thermal environment: A remote sensing study of

Guangzhou, South China. Remote Sensing, 4: 2033-2056. doi:10.3390/rs4072033.

Xu, C., and Zhang, Y. (2017). Impacts of urban surface characteristics on spatiotemporal pattern of land surface temperature in Kunming of China. *Sustainable Cities and Society* 32 (July): 87–99. doi:10.1016/j.scs. 2017.03.013.

Zha, Y., Gao, J., Ni, S. (2003). Use of normalized difference built-up index in automatically mapping urban areas from tm imagery. *International Journal of Remote Sensing 24*(3): 583–594. doi: 10.1080/01431160304987.

Zhang, Y., Odeh, I.O.A., Han, C. (2009). Bi-temporal characterization of land surface temperature in relation to impervious surface area, NDVI and NDBI, using a sub-pixel image analysis. *International Journal of Applied Earth Observation and Geoinformation* 11 (2009): 256–264. doi:10.1016/j.jag.2009.03.00.